Simulation and analysis of 1300-nm $In_{0.4}Ga_{0.6}As_{0.986}N_{0.014}/GaAs_{1-x}N_x$ quantum-well lasers with various $GaAs_{1-x}N_x$ strain compensated barriers

Yi-An Chang[a], Hao-Chung Kuo*[a] Ya-Hsien Chang[a], Shing-Chung Wang[a], Li-Hong Laih[b]
[a]Institute of Electro-Optical Engineering, National Chiao-Tung Univerisyt, Hsinchu 300, Taiwan;
[b]Millennium Communication Corporation, Hsinchu Industrial Park, Hsinchu Hsien 303, Taiwan

ABSTRACT

In this article, the laser performance of the 1300-nm $In_{0.4}Ga_{0.6}As_{0.986}N_{0.014}/GaAs_{1-x}N_x$ quantum well lasers with various $GaAs_{1-x}N_x$ strain compensated barriers (x=0%, 0.5%, 1%, and 2%) have been numerically investigated with a laser technology integrated simulation program. The simulation results suggest that with x=0% and 0.5% can have better optical gain properties and high characteristic temperature coefficient T_0 values of 110 K and 94 K at the temperature range of 300-370 K. As the nitrogen composition in GaAs1-xNx barrier increases more than 1% the laser performance degrades rapidly and the T_0 value decreases to 87 K at temperature range of 300-340 K. This can be attributed to the decrease of conduction band carrier confinement potential between $In_{0.4}Ga_{0.6}As_{0.986}N_{0.014}$ QW and $GaAs_{1-x}N_x$ barrier and the increase of electronic leakage current. Finally, the temperature dependent electronic leakage current in the $InGaAsN/GaAs_{1-x}N_x$ quantum-well lasers are also investigated.

Keywords: III-V semiconductor, InGaAsN, strain compensate, numerical simulation

1. INTRODUCTION

The InGaAsN quantum-well (QW) laser diodes (LDs) on GaAs substrate have demonstrated excellent lasing characteristics for 1300 nm semiconductor lasers, which are comparable to or superior to some of the best published results based on the conventional InP technology [1–11]. High-temperature operation has been anticipated in these material systems due to better electron and hole confinement as a result of increased band offsets and a more favorable band-offset ratio. Previous research showed that for pulse operation of InGaAsN QW LDs, the characteristic temperature coefficients T_0 value of exceeding 200 K were demonstrated [17–19] while for continue-wave (CW) operation, the T_0 of 70-110 K were also obtained [20–24]. Unfortunately, these high performance InGaAsN QW LDs showed only a slight improvement in T_0 values over those achievable by the conventional InP technology. Fehse *et al.* found that the unexpected low T_0 value of InGaAsN lasers is attributed to the existence of large Auger recombination [25]. The difficulty of nitrogen atoms incorporating into InGaAs alloys, which leads to poor crystal quality, and the hole leakage problem [26] might be the key issues that result in the unexpected low T_0 value of InGaAsN lasers. In addition, there have been several works investigating the InGaAsN QW LDs with strain-compensated GaAsN as direct barriers, which however, is a smaller band gap material system. Using GaAsN barrier instead of GaAs barrier could also reduce nitrogen outdiffusion from the well and balancing the highly compressive strain in InGaAsN QW [27]. The same phenomenon had also numerically obtained by Fan *et al* [28]. However, adding more nitrogen atoms into barrier may decrease barrier potential and the carrier leakage problem follows at high device temperature, even though longer wavelength emission can be obtained.

In this article, the laser performance of $In_{0.4}Ga_{0.6}As_{0.986}N_{0.014}/GaAs_{1-x}N_x$ QW lasers with various $GaAs_{1-x}N_x$ strain compensated barrier (x=0%, 0.5%, 1%, and 2%) are numerically investigated with a laser technology integrated program (LASTIP). It is shown that, in addition to the crystal quality of InGaAsN well layer during crystal growth, the nitrogen composition of $GaAs_{1-x}N_x$ strain compensated barrier also plays an important role in the characteristic temperature coefficient T_0 of lasers performance. Furthermore, the phenomenon of electronic leakage current with various nitrogen composition in $GaAs_{1-x}N_x$ barrier of InGaAsN QW lasers are also numerically investigated with the LASTIP simulation program.

2. METHOD AND STRUCTURE

Semiconductor Lasers and Applications II, edited by Jian-quan Yao, Yung Jui Chen, Seok Lee, Proceedings of SPIE Vol. 5628 (SPIE, Bellingham, WA, 2005) · 0277-786X/05/$15 · doi: 10.1117/12.577321

Based on the $k \cdot p$ theory with valence band mixing effect, a 8×8 Hamiltonian of the Luttinger-Kohn type and an envelope function approximation are used to solve the InGaAsN/GaAsN QW subband structures. The method is followed by Chuang [29]. The optical gain of InGaAsN/GaAsN QW structures is calculated using the Coulomb enhanced gain spectral function:

$$g(\hbar w) = real\left\{\int_{E_{g0}}^{\infty} \frac{g_0(E_{cv})}{1-q_1(E_{cv},\hbar w)}\left[1-i\frac{E_{cv}-\hbar w}{\Gamma_{cv}}\right]L(\hbar w - E_{cv})dE_{cv}\right\}, \quad (1)$$

in which

$$q(E_{cv},\hbar w) = \frac{-ia_0E_0E_{cv}}{\pi k\left|M_{ji}(E_{cv})\right|}\int_0^{\infty} dk'\,k'\frac{\left|M_{ji}(E_{cv'})\right|}{E_{cv'}} \times \frac{f_e(E_{cjk'})+f_h(E_{vjk'})-1}{\Gamma_{cv}+i(E_{cv}-\hbar w)} \times \Theta(k,k'), \quad (2)$$

$$\Theta(k,k') = \int_0^{2\pi} d\theta \frac{1+C_{pl}ka_0q^2/32\pi N_{2D}}{1+q/k+C_{pl}ka_0qk^3/32\pi N_{2D}}, \quad q^2 = k^2+k'^2-2kk'\cos\theta, \quad (3), (4)$$

and θ is the angle between in-plane vectors k and k'. $g_0(E_{cv})$ is the spectral wave function, which consists of a sum of $g_{ji}(E_{cv})$ contributions from transitions between jth-subband electrons and ith-subband holes. Γ_{cv} represents the Lorenzian width and equals to $\hbar/\tau_{cv}$, which is simplified without considering the dependence upon $\hbar w$ and E_{cv} energies in our calculations. a_0 is exciton Bohr radius given by $4\pi\hbar^2\varepsilon_b\varepsilon_0/e^2m_{rj}$. E_0 is the corresponding Rydberg energy and E_{cv} is specified by $E_{cv}(k) = E_g + \Delta E_g + E_{cjk} + E_{vik}$ where E_{cjk} and E_{vik} are electron and hole energies from jth-subband of conduction and ith-subband of valence band quantum well in the active region. $\left|M_{ji}\right|^2$ is the transition matrix element and C_{pl} is a unitless constant typically in a range 1-4. $N_{2D} = n \times$ (quantum well thickness) is the two-dimensional carrier density in a quantum well. The gain spectral is broadened by the Lorenzian function [30].

For this specific simulation, the ratio of conduction band to valence band offset is estimated to 0.7/0.3 [31]. The bandgap energy of $In_{1-x}Ga_xAs_yN_{1-y}$ material at room temperature (RT, 300 K) is governed by the following bilinear terms with two bowing terms:

$$E_g(term1) = x\cdot y\cdot E_{g,GaAs} + x\cdot(1-y)\cdot E_{g,GaN}, \quad (5)$$

$$E_g(term2) = (1-x)\cdot y\cdot E_{g,InAs} + (1-x)\cdot(1-y)\cdot E_{g,InN}, \quad (6)$$

$$E_g(bowing) = x\cdot b\_GaAsN\cdot y\cdot(1-y) + y\cdot b\_InGaAs\cdot x\cdot(1-x), \quad (7)$$

where x and y denote the gallium and arsenide compositions in InGaAsN alloy, and the bandgap energies of GaAs, InAs, GaN and InN are 1.424, 0.355, 3.42 and 0.77 [32] eV. The bowing parameters for GaAsN and InGaAs ternary alloys are -18 [33] and -0.6 eV. The temperature dependent bandgap energy is as follows:

$$E_g(T) = -5.5\times10^{-4}\cdot\left[\frac{T^2}{T+225} - \frac{300^2}{300+225}\right], \quad (8)$$

where $E_g(T)$ is the bandgap energy of InGaAsN alloy at temperature T. Therefore, the temperature dependent bandgap energy of InGaAsN alloy is

$$E_g(InGaAsN) = E_g(term1) + E_g(term2) + E_g(bowing) + E_g(T). \quad (9)$$

The effective mass of electrons used in simulation is as follow:

$$m_e(term1) = x\cdot y\cdot m_{e,GaAs} + x\cdot(1-y)\cdot m_{e,GaN}, \quad (10)$$

$$m_e(term2) = (1-x)\cdot y\cdot m_{e,InAs} + (1-x)\cdot(1-y)\cdot m_{e,InN}, \quad (11)$$

$$m_e(InGaAsN) = m_e(term1) + m_e(term2), \quad (12)$$

where the effective mass of electrons in GaAs, InAs, GaN and InN are $0.064\times m_0$, $0.023\times m_0$, $0.2\times m_0$ and $0.11\times m_0$ respectively. The effective masses of light holes (LH) and heavy-holes (HH) are governed by the same form in Eq. (6), and the effective masses of light holes and heavy holes for GaAs are $0.09\times m_0$ and $0.377\times m_0$, $0.027\times m_0$ and $0.263\times m_0$ for InAs, $0.9767\times m_0$ and 1.3758 for GaN, and $0.5133\times m_0$ and $1.5948\times m_0$ for InN respectively. The Auger coefficients for InGaAsP and InGaAsN are 3.5×10^{-42} and 1.5×10^{-41} m^2/s. Other material-dependent parameters are also taken from the default database values given in the LASTIP material macro file [30].

A schematic diagram of the preliminary InGaAsN / GaAsN ridge LD structure under this study is shown in Fig. 1. It is assumed that the InGaAsN ridge LD structure is grown on 100-μm-thick n-type GaAs substrate with doping concentration of 5×10^{18} cm^{-3} and a GaAs layer with thickness of 100 nm and n-doping concentration of 5×10^{18} cm^{-3}. A 150-nm-thick lower AlGaAs cladding layer of aluminum grading from 0.3 to 0 and n-doping concentration of 2×10^{18} cm^{-3} is grown on top of the GaAs layer, followed by a 100-nm-thick GaAs optical confinement layer with n-doping concentration of 2×10^{18} cm^{-3}. The undoped active region consists of single InGaAsN QW that is sandwiched between two GaAsN barriers. On top of the active region is a p-type GaAs optical confinement layer with doping concentration of 5×10^{17} cm^{-3}, and a 150-nm-thick upper AlGaAs cladding layer of aluminum grading from 0 to 0.3 with p-doping concentration of 5×10^{17} cm^{-3}. Finally, a 100-nm-thick GaAs layer with p-doping concentration of 1×10^{19} cm^{-3} is capped to complete the structure.

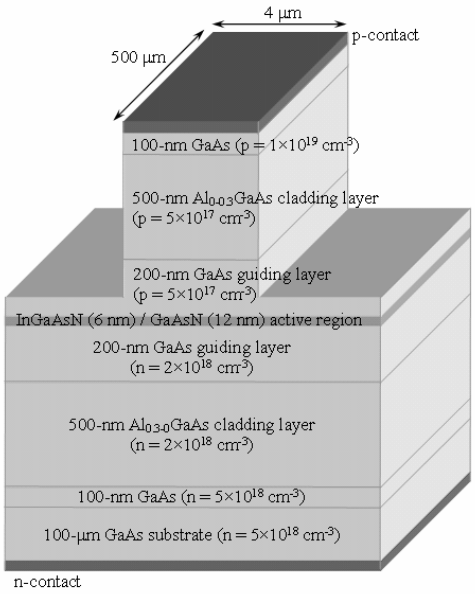

Figure 1: Schematic diagram of the preliminary InGaAsN/GaAsN ridge LD structure under study.

The n-contact is assumed to locate on bottom of the n-type GaAs bottom layer and the p-contact is located on top of the p-type GaAs capping layer. The thickness of InGaAsN QW and GaAsN barrier are 6 and 12 nm, respectively. The ridge waveguide is 4 μm in width and 500 μm in length. Two end facets are assumed to anti-reflection and high-reflection coating that provide 20% and 98% reflectivity. Background loss of 30 cm^{-1} and thermal conductivity of 40 Wm/K for InGaAsN material are assumed in the simulation.

3. TEMPERATURE DEPENDENT OPTICAL GAIN PROPERTIES

Temperature effects on the optical gain properties of $In_{0.4}Ga_{0.6}As_{0.986}N_{0.014}$ and $In_{0.8}Ga_{0.2}As_{0.69}P_{0.31}$ QW materials are studied in the first instance. For the purpose of obtaining an emission wavelength of 1.3 μm, the nitrogen composition in InGaAsN / GaAs active region is 1.4% when the indium composition in InGaAsN QW is 0.4. Figure 2 shows the material gains of RT $In_{0.4}Ga_{0.6}As_{0.986}N_{0.014}$ and $In_{0.8}Ga_{0.2}As_{0.69}P_{0.31}$ QW materials at an input carrier concentration of 2×10^{18} cm^{-3}. The barrier materials used under this study for $In_{0.4}Ga_{0.6}As_{0.986}N_{0.014}$ and $In_{0.8}Ga_{0.2}As_{0.69}P_{0.31}$ QW materials are $GaAs_{1-x}N_x$ with x=0%, 0.5%, 1%, 2% and $In_{0.9}Ga_{0.1}As_{0.24}P_{0.76}$ [34]. It is clear

that $In_{0.4}Ga_{0.6}As_{0.986}N_{0.014}$ / $GaAs_{1-x}N_x$ (x=0%, 0.5%, 1%, 2%) materials have higher maximum material gains than that of InGaAsP material. The highest maximum material gain is obtained when x=0%, i.e. GaAs barrier, and the maximum material gain is found to be red shift from 1.3 to 1.34 μm by increasing x value from 0% to 2% in $GaAs_{1-x}N_x$ barrier. In addition, the maximum material gain decreases rapidly with increasing x value in $GaAs_{1-x}N_x$ barrier as a result of the decrease of conduction band carrier confinement potential. Nevertheless, the maximum material gain of $In_{0.4}Ga_{0.6}As_{0.986}N_{0.014}/GaAs_{1-x}N_x$ is twice approximately higher than that of $In_{0.8}Ga_{0.2}As_{0.69}P_{0.31}/In_{0.9}Ga_{0.1}As_{0.24}P_{0.76}$ when the input carrier concentration is 2×10^{18} cm^{-3}.

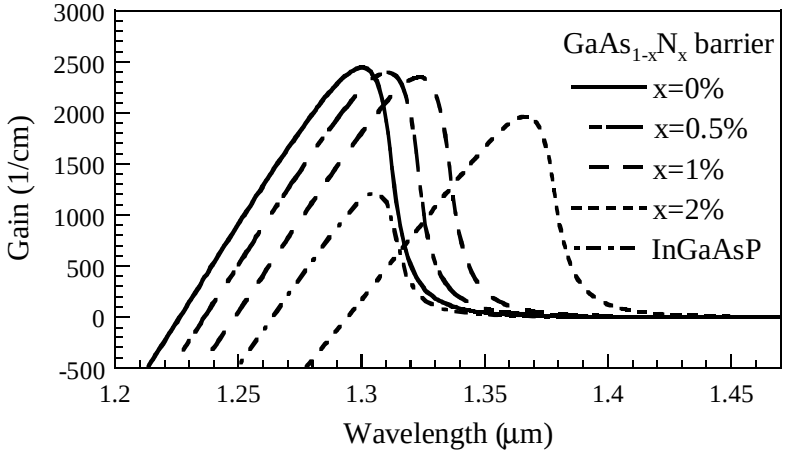

Figure 2: Material gains of RT $In_{0.4}Ga_{0.6}As_{0.986}N_{0.014}$ and $In_{0.8}Ga_{0.2}As_{0.69}P_{0.31}$ QW materials at an input carrier concentration of 2×10^{18} cm^{-3}.

The maximum material gain of using $GaAs_{1-x}N_x$ barriers with x=0%, 0.5%, 1% and 2% as a function of temperature are shown in Fig. 3. The maximum material gain drops almost linearly with increasing temperature. A red shift of the maximum material gain with x=0% from 1.3 to 1.35 μm and the decrease of the maximum material gain value from 2443 to 1575 cm^{-1}, which is due to the wider spreading of the Fermi distribution of carriers and stronger Auger recombination losses, are numerically obtained when the temperature increases from 300 to 370 K. Manifestly, the severe decrease of the maximum material gain value caused by the linear increase of x value indicates that increasing nitrogen composition in GaAsN barrier may procure the poor laser performance as a result of the relatively low material gain.

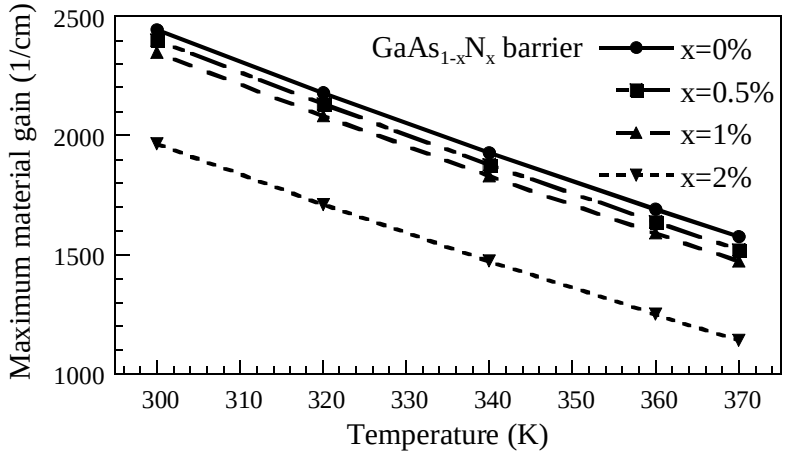

Figure 3: Maximum material gain of using $GaAs_{1-x}N_x$ barriers with x=0%, 0.5%, 1% and 2% as a function of temperature.

Figure 4 shows the transparency carrier concentration as a function of temperature when using $GaAs_{1-x}N_x$ barriers with x=0%, 0.5%, 1% and 2%. The gain increases with input carrier concentration and the RT transparency carrier concentrations of $In_{0.4}Ga_{0.6}As_{0.986}N_{0.014}$ /$GaAs_{1-x}N_x$ materials are noticeably lower than that of $In_{0.8}Ga_{0.2}As_{0.69}P_{0.31}$ / $In_{0.9}Ga_{0.1}As_{0.24}P_{0.76}$ material, 1.35×10^{18} cm^{-3}. The differential gains of $In_{0.4}Ga_{0.6}As_{0.986}N_{0.014}$ / $GaAs_{1-x}N_x$ materials are also higher than that of $In_{0.8}Ga_{0.2}As_{0.69}P_{0.31}$ / $In_{0.9}Ga_{0.1}As_{0.24}P_{0.76}$ material due to the fact that $In_{0.4}Ga_{0.6}As_{0.986}N_{0.014}$ /$GaAs_{1-x}N_x$ based material has relatively high conduction band offset and more electrons can be confined in the active layer effectively. The transparency carrier concentrations at RT of using $GaAs_{1-x}N_x$ barriers with x=0% and x=2% are 9.8×10^{17} and 1.06×10^{18} cm^{-3} respectively. For x=0%, the transparency carrier concentration increases almost linearly to 1.25×10^{18} cm^{-3} when the temperature is 370 K. The transparency carrier concentrations of using $GaAs_{1-x}N_x$ barriers with x=0.5% and 1% are slightly higher than that of GaAs barrier in a temperature range of 300-370 K. However, the transparency carrier concentration increases apparently when the x value is 2% and it increases rapidly when the temperature is higher than 350 K.

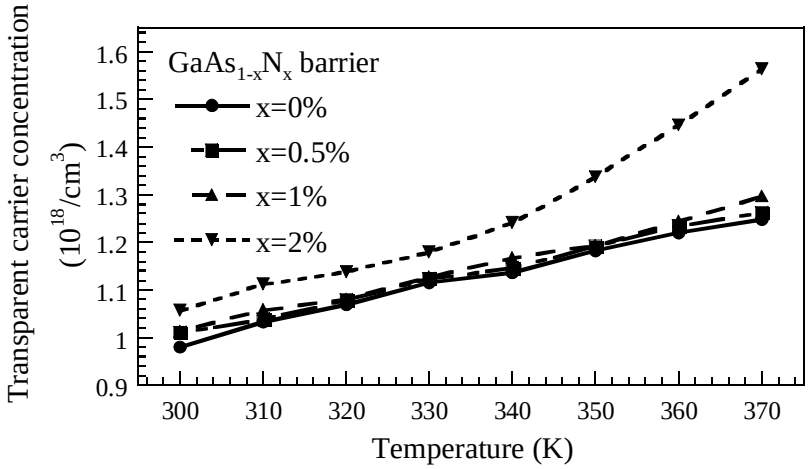

Figure 4: Transparency carrier concentration as a function of temperature when using $GaAs_{1-x}N_x$ barriers with x=0%, 0.5%, 1% and 2%.

From the analysis of the optical gain properties of $In_{0.4}Ga_{0.6}As_{0.986}N_{0.014}$ QW sandwiched between $GaAs_{1-x}N_x$ barriers with variant x values, we find that using $GaAs_{1-x}N_x$ barriers with x value ranging from zero to 1% can have better temperature dependent optical gain properties. When the x value increases to 2%, the maximum material gain and the transparency carrier concentration abate remarkably. It indicates that $In_{0.4}Ga_{0.6}As_{0.986}N_{0.014}$ QW sandwiched between $GaAs_{1-x}N_x$ barriers may have better laser performance, i.e. lower threshold current density and higher slope efficiency, when the x value is zero or less than 2%. Especially, using high potential GaAs barrier provides better electron confinement and results in obtaining highest material gain and lowest transparency carrier concentration. A highest T_0 value may also be obtained as a result of reducing the probability of electronic leakage current if the LD structure is under high temperature operation. Besides, after the consideration of using GaAsN barrier instead of GaAs barrier has several advantages in experiment and longer wavelength can easier be obtained, we find in this study that using $GaAs_{1-x}N_x$ barriers with x=0.5% and 1% can also provide high material gain and low transparency carrier concentration.

4. L-I CHARACTERISTIC AND ELECTRONIC LEAKAGE CURRENT

The thermal heating effects are quite important and need to be incorporated for the discussion of L-I characteristic in a LD structure. For the preliminary LD structure under study, the heat sources, which are separated into Joule heat, optical recombination heat, Thomson and Peltier heating terms, are considered in our simulation. Figure 5 shows the *L-I* characteristics of $In_{0.4}Ga_{0.6}As_{0.986}N_{0.014}$ QW sandwiched between $GaAs_{1-x}N_x$ barriers with x=0%, 0.5% and 1.0% in a device temperature range of 300-370 K. The threshold current of using $GaAs_{1-x}N_x$ barrier with x=0% increases from 37 to 70 mA and the slope efficiency decreases from 0.302 to 0.185 W/A when the device temperature increases

from 300 to 370 K. However, we find in Figs. 5(b) and 5(c) that the laser performance becomes poorer when the x value increases to 0.5% and 1.0%, even thought the optical gain properties of x=0.5% and x=1.0% are only slightly worse than GaAs barrier, as mentioned in Figs. 3 and 4. For x=0.5%, the threshold current increases from 52 to 89 mA when the device temperature increases from 300 to 350 K and no lasing is observed when the device temperature is higher than 360 K. For x=1%, the population inversion is more difficult to achieve and the threshold current increases rapidly from 58 to 91 mA when the device temperature increases from 300 to 340 K. No lasing is observed when the device temperature is higher than 340 K.

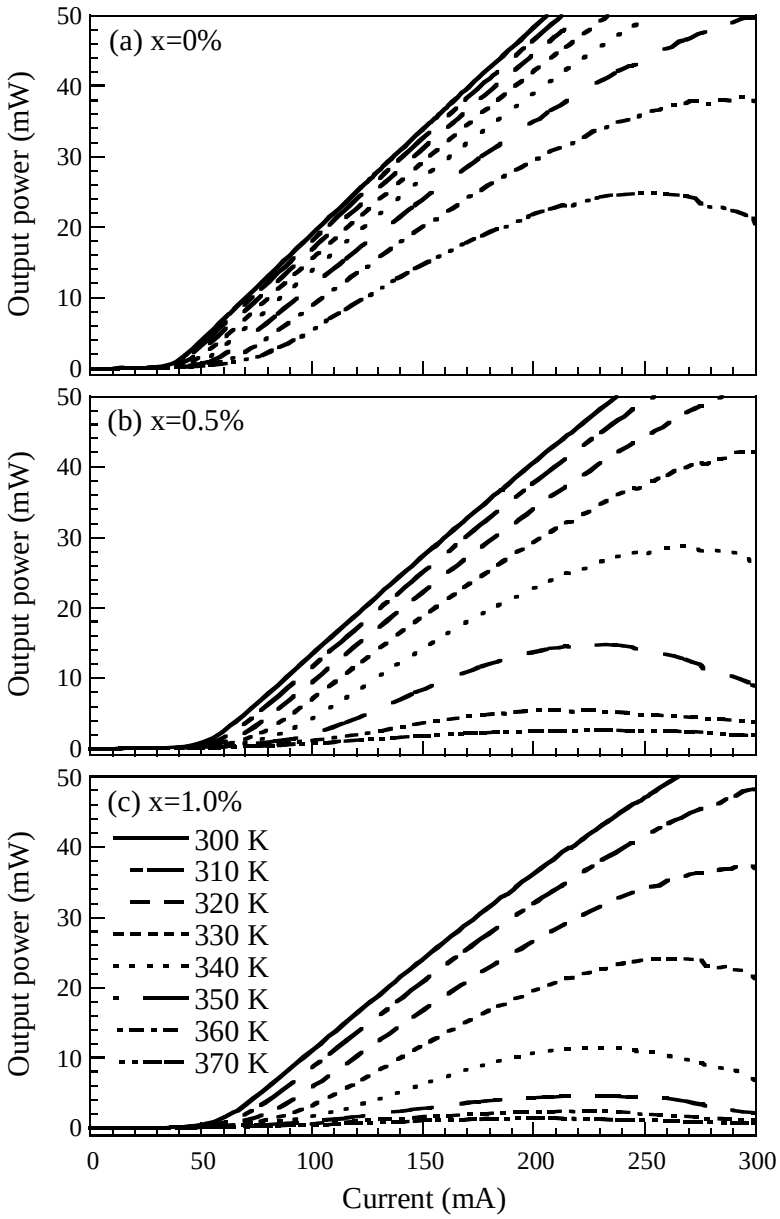

Figure 5: *L-I* characteristics of $In_{0.4}Ga_{0.6}As_{0.986}N_{0.014}$ QW sandwiched between $GaAs_{1-x}N_x$ barriers with (a) x=0%, (b) 0.5% and (c) x=1.0% in a device temperature range of 300-370 K.

Figure 6 depicts the threshold currents of using $GaAs_{1-x}N_x$ barriers with x=0%, 0.5% and 1.0% as a function of the device temperature. The T_0 value of using GaAs barrier obtained in this study in a device temperature range of 300-370 K is 110 K. When using $GaAs_{1-x}N_x$ barriers with x=0.5% and 1%, the T_0 values are 94 and 87 K,

respectively. The simulation results indicate that the laser performance becomes poorer and the T_0 value decreases rapidly when the x value in $GaAs_{1-x}N_x$ barrier increases from zero to 1%. This can be due to that adding more nitrogen composition in $GaAs_{1-x}N_x$ barrier results in the smaller conduction band carrier confinement potential and the electronic current leakages to the p-type layers effortlessly. Therefore the laser performance decreases rapidly when the device temperature increases.

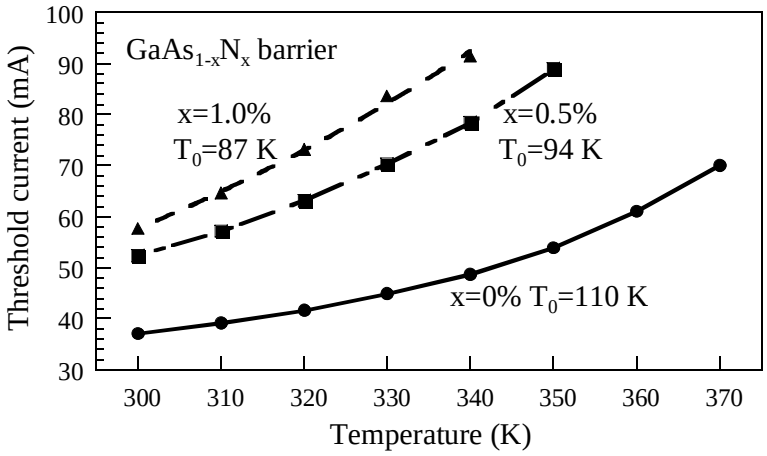

Figure 6: Threshold currents of using $GaAs_{1-x}N_x$ barriers with x=0%, 0.5% and 1.0% as a function of the device temperature.

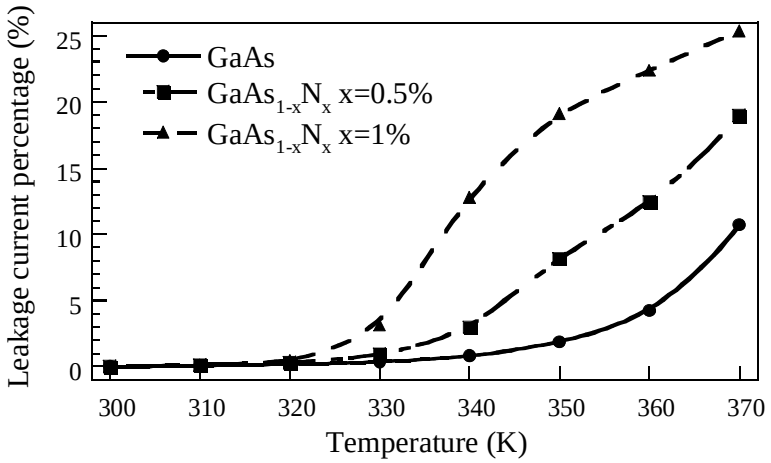

Figure 7: Percentage of electronic leakage current as a function of the device temperature when the $In_{0.4}Ga_{0.6}As_{0.986}N_{0.014}$ QW is sandwiched between $GaAs_{1-x}N_x$ barriers with x=0%, 0.5% and 1% at an input current of 300 mA.

Figure 7 depicts the percentage of electronic leakage current as a function of the device temperature when the $In_{0.4}Ga_{0.6}As_{0.986}N_{0.014}$ QW is sandwiched between $GaAs_{1-x}N_x$ barriers with x=0%, 0.5% and 1% at an input current of 300 mA. Specifically, more and more electrons overflow to the p-type layers and do not contribute to the stimulated emission when the x value in $GaAs_{1-x}N_x$ barriers increases. Using GaAs barrier provides relatively high conduction band carrier confinement potential and in turn reduces the probability of electronic current overflowing to the p-type layers in a device temperature range of 300-370 K. Most electronic current can be confined in active layer effectively when the device temperature is in a range of 300-340 K; however, when the device temperature is 350 K or higher the percentage of electronic leakage current increases and it reaches to 10.7% when the device temperature raises to 370 K. For x=0.5% and 1.0%, the percentages of electronic leakage current are negligibly small when the device

temperature is below 320 K. The percentage of electronic leakage current of x=0.5% increases from 1% to 19% with the temperature increases from 330 to 370 K. For x=1%, it already has 3% electronic leakage current when the device temperature is 330 K and more than 13% electronic current overflows to the p-type layers when the device temperature is higher than 340 K. It is noteworthy to mention that the $In_{0.4}Ga_{0.6}As_{0.986}N_{0.014}$ / $GaAs_{1-x}N_x$ LD does not lase when the percentage of electronic leakage current is higher than 13%.

5. CONCLUSION

In summary, the temperature dependent optical gain properties, laser performance and the electronic leakage current of $In_{0.4}Ga_{0.6}As_{0.986}N_{0.014}$ QW laser with various $GaAs_{1-x}N_x$ strain compensated barrier have been numerically analyzed for the first time. It is shown that, the nitrogen composition of $GaAs_{1-x}N_x$ strain compensated barriers play an important role in the characteristic temperature coefficient T_0 value. The simulation results also suggest that using $GaAs_{1-x}N_x$ strain-compensated barriers with x value less than 0.5% may provide better optical gain properties and higher T_0 value. No lasing is observed when the percentage of the electronic leakage current is higher than 13%.

ACKNOWLEDGMENTS

The authors would like to give the sincere appreciation to the Crosslight incorporation for providing the advanced two-dimensional LASTIP simulation program (version 2003.12) and Prof. Nelson Tansu in Leigh University, USA for the precious discussion. This work is supported by the National Science Council, Republic of China, under grant NSC-90-2215 -E009-088 and by the Academic Excellence Program of the Ministry of Education of ROC under the contract NO. 88-FA06-AB.

REFERENCES

1. S. F. Yu, in: Analysis and Design of Vertical cavity Surface Emitting Lasers, John Wiley & Sons, Inc, Hoboken, New Jersey, 2003.
2. S. Sato, and S. Satoh, *J. Cryst. Growth* **192**, 381, 1998.
3. D. Gollub, Moses S, Fischer M, and Forchel A, *J. Cryst. Growth* **251**, 353, 2003.
4. Mazzucato S, Balkan N, Teke A, Erol A, Potter RJ, Arikan MC, Marie X, Fontaine C, Carrere H, Bedel E, and Lacoste G, *J. Appl. Phys.* **93**, 2440, 2003.
5. Sun HD, Dawson MD, Othman M, Yong JCL, Rorison JM, Gilet P, Grenouillet L, and Million A, *Appl. Phys. Lett.* **82**, 376, 2003.
6. Henning Riechert, Arun Ramakrishnan, and Gunther Steinle, *Semicond. Sci. Technol.* **17**, 892, 2002.
7. W. Li, M. Pessa, T. Ahlgren, J. Decker, *Appl. Phys. Lett*. **79**, 1094, 2001.
8. N. Tansu, and Luke J. Mawst, *IEEE Photonics Technol. Lett*. **14**, 1052, 2002.
9. J.C.L. Yong, J. M. Rorison, M. Othman, H. D. Sun, M. D. Dawson, and K.A. Willaims, *IEE Proc.-Optoelectron.* **150**, 80, 2003.
10. J. C. L. Yong, Judy. M. Rorison, and Ian H. White, *IEEE J. Quantum Electron.* **38**, 1553, 2002.
11. D. Alexandropoulos, and M.J. Adams, *IEE Proc.-Optoelectron.* **150**, 40, 2003.
12. G. Steinle, F. Mederer, M. Kicherer, R. Michalzik, G. Kristern, A. Y. Egorov, H. Riechert, H. D. Wolf, and K. J. Ebeling, *Electron. Lett*. **37**, 632, 2001.
13. Y. -L. Chang, T. takeuchi, M. Leary, D. Mars, A. Tandon, R. Twist, S. Belov, D. Bour, M. Tan, D. Roh, Y. -K, Song, L. Mantese, and H. -C. Luan, *Electrochemical Society Proc*. **2003-11**, 33, 2003.
14. N. Tansu, Andrew Quandt, Manoj Kanskar, Willaim Mulhearn, and Luke J. Mawst, *Appl. Phys. Lett.* **83**, 18, 2003.
15. M. R. Gokhale, P. V. Studenkov, J. Wei, and S. R. Forrest, *IEEE Photonics Technol. Lett.* **12**, 131, 2000.
16. B. Borchert, A. Yu. Egorov, S. Illek, M. Komainda, and H. Riechert, *Electron. Lett.* **35**, 2204, 1999.
17. W. J. Fan, S. T. Ng, S. F. Yoon, M. F. Li, and T. C. Chong, *J. Appl. Phys*. **93**, 5836, 2003.
18. Shunichi Sato, *Jpn. J. Appl. Phys*. **39**, 3403, 2000.

19. Takeshi Kitatani, Kouji Nakahara, Masahiko Kondow, Kazuhisa Uomi, and Toshiaki Tanaka, *Jpn. J. Appl. Phys.* **39**, L86, 2000.
20. N. Tansu, and L. J. Mawst, *IEEE Photonics Technol. Lett*. **14**, 444, 2002.
21. N. Tansu, N. J. Kirsch, and L. J. Mawst, *Appl. Phys. Lett*. **81**, 2523, 2002.
22. C. S. Peng, T. Jouhti, P. Laukkanen, E.-M. Pavelescu, J. Konttinen, W. Li, and M. Pessa, *IEEE Photonics Technol. Lett.* **14**, 275, 2002.
23. D. A. Livshits, A. Yu. Egorov, and Riechert, *Electron. Lett*. **36**, 1381, 2000.
24. J. Wei, F. Xia, C. Li, and S. R. Forrest, *IEEE Photonics Technol. Lett.* **14**, 597, 2002.
25. R. Fehse, S. Tomic, A. R. Adams, S. J. Sweeney, E. P. O'Reilly, and A., H. Riechert, *IEEE J. Sel. Top. Quantum Electron*. **8**, 801, 2002.
26. N. Tansu, and L. J. Mawst, *Appl. Phys. Lett*. **82**, 1500, 2003.
27. Wei Li, Tomi Jouhti, Chang Si Peng, Janne Konttinen, Pekka Laukkanen, Emil-Mihai Pavelescu, Mihail Dumitrescu, and Markus Pessa, *Appl. Phys. Lett.* **79**, 3386, 2001.
28. W. J. Fan, S. T. Ng, S. F. Yoon, M. F. Li, and T. C. Chong, *J. Appl. Phys*. **93**, 5836, 2003.
29. S. L. Chuang, *Phys. Rev. B* **43**, 9649, 1991.
30. LASTIP User's Manual Version 2003.12 Crosslight Inc Software, Canada. Available online at web page http://www.crosslight.ca.
31. L. Bellaiche, S.-H. Wei, and A. Zunger, *Phys. Rev. B* **54**, 17568**,** 1996.
32. J. Wu, W. Walukiewicz, K.M. Yu, J.W. Ager III, E.E. Haller, H. Lu, and W.J. Schaff, *Appl. Phys. Lett*. **80**, 4741, 2002.
33. M. Kondow, K. Uomi, A. Niwa, T. Kitatani, S. Watahiki, and Y. Tazawa, *Jpn. J. Appl. Phys*. **35**, 1273 , 1996.
34. Alistair F. Phillips, Stephen J. Sweeney, Alfred R. Adams, and Peter J. A. Thijs, *IEEE J. Sel. Top. Quantum Electron.* **5**, 401, 1999.

* hckuo@faculity.nctu.edu.tw; phone 886 3 571-2121 ext. 31986; fax 886 3 571-6631; Institute of Electro-Optical Engineering, National Chiao-Tung, Hsinchu 300, Taiwan